East Asian Journal on Applied Mathematics
doi: 10.4208/eajam.030616.130517a

Vol. 7, No. 3, pp. 566-582
August 2017

# Spike-Layer Simulation for Steady-State Coupled Schrödinger Equations

Liming Liao, Guanghua Ji*, Zhongwei Tang and Hui Zhang

*Laboratory of Mathematics and Complex Systems, Ministry of Education and School of Mathematical Sciences, Beijing Normal University, Beijing 100875, China.*

*Received 3 June 2016; Accepted (in revised version) 13 May 2017.*

**Abstract.** An adaptive finite element method is adopted to simulate the steady state coupled Schrödinger equations with a small parameter. We use damped Newton iteration to solve the nonlinear algebraic system. When the solution domain is elliptic, our numerical results with Dirichlet or Neumann boundary conditions are consistent with previous theoretical results. For the dumbbell and circular ring domains with Dirichlet boundary conditions, we obtain some new results that may be compared with future theoretical analysis.

**AMS subject classifications**: 33F05, 68U20
**Key words**: Schrödinger equations, damped Newton iteration, adaptive finite element method, spike-layer solution.

## 1. Introduction

Nonlinear Schrödinger equations model a wide range of problems in physics, such as particle movement and Bose-Einstein condensation. If $\Omega$ denotes a bounded domain in two-dimensional or three-dimensional space, we consider the following two coupled Schrödinger equations in $H^1(\Omega)\times H^1(\Omega)$:

$$\begin{cases} -\varepsilon^2\triangle u+u=\mu_1 u^3+\beta v^2 u, \\ -\varepsilon^2\triangle v+v=\mu_2 v^3+\beta u^2 v, \\ \quad u,v>0 \ in\ \Omega, \end{cases} \tag{1.1}$$

subject to either Dirichlet boundary conditions

$$u=v=0 \ \ on \ \ \partial\Omega \tag{1.2}$$

or Neumann boundary conditions

$$\frac{\partial u}{\partial n}=\frac{\partial v}{\partial n}=0 \ \ on \ \ \partial\Omega, \tag{1.3}$$

*Corresponding author. *Email address:* ghji@bnu.edu.cn (G. Ji)

 ©2017 Global-Science Press

https://doi.org/10.4208/eajam.030616.130517a Published online by Cambridge University Press

where $\triangle = \sum_{i=1}^{N} \partial^2/\partial x_i^2$ is the Laplace operator, $\Omega$ is a bounded open domain in $\mathbb{R}^2$ with a smooth boundary $\partial\Omega$, $\varepsilon$ is a positive parameter, $\mu_1$ and $\mu_2$ are positive constants, $\beta \in \mathbb{R}$ is also a constant, and $n$ denotes the unit outward normal at $x \in \partial\Omega$. The corresponding energy functional is

$$J_\varepsilon(u,v) = \frac{1}{2}\int_\Omega \left[\varepsilon^2|\nabla u|^2 + u^2 + \varepsilon^2|\nabla v|^2 + v^2\right] dx - \frac{1}{4}\int_\Omega (\mu_1 u^4 + \mu_2 v^4 + 2\beta v^2 u^2)\, dx\,, \quad (1.4)$$

and solutions of the system (1.1) correspond to critical points of $J_\varepsilon$ — i.e. $\nabla J_\varepsilon(u,v) = \mathbf{0}$, where $\nabla J$ is the Fréchet derivative. Since there is a canonical identification between a Hilbert space and its dual, we always identify the Fréchet derivative with its canonical dual. As in Ref. [4], we consider the Nehari manifold

$$N(\varepsilon,\Omega) = \left\{ \begin{array}{l} (u,v) \in H^1(\Omega)\times H^1(\Omega)\,,\, u \gneqq 0\,,\, v \gneqq 0\,: \\ \displaystyle\int_\Omega \left[\varepsilon^2|\nabla u|^2 + u^2\right] dx = \int_\Omega [\mu_1 u^4 + \beta u^2 v^2]\, dx \\ \displaystyle\int_\Omega \left[\varepsilon^2|\nabla v|^2 + v^2\right] dx = \int_\Omega [\mu_1 v^4 + \beta u^2 v^2]\, dx \end{array} \right\}. \quad (1.5)$$

Any nontrivial positive solution of (1.1) in $H^1(\Omega)\times H^1(\Omega)$ belongs to the manifold (1.5). Among the nontrivial positive solutions, the one or more with the least energy are called the least energy solutions. The least energy solutions of the system (1.1) are minimums of $J_\varepsilon$ on $N(\varepsilon,\Omega)$ — i.e.

$$c_\varepsilon = \inf_{(u,v)\in N(\varepsilon,\Omega)} J_\varepsilon(u,v)\,.$$

The system (1.1) arises in the Hartree-Fock theory for a double condensate — i.e. a binary mixture of Bose-Einstein condensates in two different hyperfine states $|1\rangle$ and $|2\rangle$ (cf. Ref. [1]). Physically, $u$ and $v$ are corresponding condensate amplitudes such that $\epsilon^2 = \hbar^2/(2m)$ and $\mu_j = -(N_j - 1)U_{jj}$ where $\hbar$ is the Planck constant, $m$ is the atom mass, and $N_j$ is a fixed number of atoms in the hyperfine state $|j\rangle$. Moreover, we have $N_1, N_2 \geq 1$, $\beta = -N_2 U_{12}$ and $U_{ij} = 4\pi\hbar^2/m\ a_{ij}$, where $a_{jj}\,(j = 1,2)$ and $a_{12}$ are the intraspecies and interspecies scattering lengths. The sign of the scattering length $a_{12}$ determines whether the interactions of states $|1\rangle$ and $|2\rangle$ are repulsive or attractive. When $a_{12} > 0$ (i.e. $\beta < 0$), the interactions of the states $|1\rangle$ and $|2\rangle$ are repulsive, and when $a_{12} < 0$ (i.e. $\beta > 0$) the interactions of the states $|1\rangle$ and $|2\rangle$ are attractive — cf. Ref. [2]. For atoms of the single state $|j\rangle$, when $a_{jj} < 0$ (i.e. $\mu_j > 0$) the interactions of the single state $|j\rangle$ are attractive.

For the case when $\varepsilon = 1\,,\ \Omega = R^2$, there are many contributions on the bound states of the system (1.1). For example, Sirakov [7] discusses when the $\beta$ problem (1.1) has or has not a least energy solution, and Wang *et al.* [12] construct an unbounded sequence of non-radial positive vector solutions of segregated type in the repulsive case and an unbounded sequence of non-radial positive vector solutions of synchronised type in the attractive case — cf. also Bartsch *et al.* [8] and Lin & Wei [4–6] on the bound states of Schrödinger systems.

When $\varepsilon$ is a random positive parameter and $\Omega$ is a bounded domain, there are also many articles on the bound states of the system (1.1). Lin & Wei [4] considered the system

https://doi.org/10.4208/eajam.030616.130517a Published online by Cambridge University Press

(1.1) subject to the Dirichlet boundary condition (1.2). They proved that a least energy solution exists by minimising the Nehari manifold for $\beta < \beta_0$ and discussed the asymptotic behaviour as $\varepsilon \to 0$, where $0 < \beta_0 < \mu_1\mu_2$ is a constant depending only on $n$. Specifically, if $dist(P, \partial\Omega)$ denotes the distance function of point P in $\Omega$ to $\partial\Omega$, they showed that when $\beta < 0$ the maximum points of the two components of the least energy solution to the system (1.1) approach different local maximum points of $dist(P, \partial\Omega)$ as $\varepsilon \to 0$, whereas when $0 < \beta < \beta_0$ the maximum points of the two components of the least energy solution approach each other as $\varepsilon \to 0$. More recently, Tang [10, 13, 14] considered the system (1.1) with the Neumann boundary condition (1.3). For any $\varepsilon > 0$, Tang [10] proved that when $\beta < \min\{\mu_1, \mu_2\}$ or $\beta > \max\{\mu_1, \mu_2\}$ the system (1.1) has a least energy solution $(u_\varepsilon, v_\varepsilon)$ that achieves $c_\varepsilon$ but when $\min\{\mu_1, \mu_2\} < \beta < \max\{\mu_1, \mu_2\}$ the system (1.1) has no solution, and discussed the asymptotic behaviour of $(u_\varepsilon, v_\varepsilon)$ as $\varepsilon \to 0$. Thus if $P_\varepsilon$ and $Q_\varepsilon$ are the respective local maximum points of $u_\varepsilon$ and $v_\varepsilon$ and $H(P)$ denotes the mean curvature on $\partial\Omega$, he proved that when $\varepsilon$ becomes sufficiently small both $P_\varepsilon$ and $Q_\varepsilon$ are located on the boundary of $\Omega$. Furthermore, when $0 \le \beta < \min\{\mu_1, \mu_2\}$ or $\beta > \max\{\mu_1, \mu_2\}$, as $\varepsilon \to 0$ $|P_\varepsilon - Q_\varepsilon|/\varepsilon \to 0$ and $H(P_\varepsilon) \to \max_{P\in\partial\Omega} H(P)$, $H(Q_\varepsilon) \to \max_{P\in\partial\Omega} H(P)$, and also $u_\varepsilon, v_\varepsilon \to 0$ in $C^1_{loc}(\bar{\Omega}\setminus\{P_\varepsilon, Q_\varepsilon\}$ — i.e. $P_\varepsilon$ and $Q_\varepsilon$ converge to the same point on the boundary, which is the maximum point of its mean curvature. For $\beta < 0$ on the other hand, when $\varepsilon \to 0$ and $|P_\varepsilon - Q_\varepsilon|/\varepsilon \to \infty$ and $P_\varepsilon \to P$ and $Q_\varepsilon \to Q$, then $P$ and $Q$ must be different maximum points of the mean curvature on the boundary except when the mean curvature of the boundary has only one maximum point. Tang [13] also showed there exist solutions to the system (1.1) with multi-peaks, where all peaks lie on the boundary of the domain and are located either near the local maxima or near the local minima of its mean curvature. He also proved the existence of segregated solutions $(u_\varepsilon, v_\varepsilon)$ such that both of $u_\varepsilon$ and $v_\varepsilon$ admit more than one local maximum; and furthermore, that as $\varepsilon \to 0$ the maximum points for $u_\varepsilon$ and $v_\varepsilon$ respectively concentrate at different local maximum or local minimum points of the mean curvature $H(P)$.

There are numerical simulations producing positive solutions of the system (1.1) for the scalar case $-\varepsilon^2\triangle u + u = u^3$, $u > 0$, $x \in \Omega$ (with $\beta = 0$) for Dirichlet or Neumann boundary conditions — cf. Refs. [3, 11, 15]. For the Dirichlet boundary condition, Chen *et al.* [3] introduced the Mountain Pass Algorithm (MPA) to obtain the interior single-peak solution on an elliptic domain when $\varepsilon \ge 10^{-1}$. Ávilaa *et al.* [15] extended the MPA idea to consider singularly perturbed problems, and developed a finite element approach combined with steepest descent calculations to obtain some interior single-peak solutions on a circular domain when $\varepsilon \ge 10^{-6}$, or on a dumbbell domain when $\varepsilon \ge 10^{-5}$. For the Neumann boundary condition, Xie *et al.* [11] developed a modified Local Maximum Method (LMM) that produced boundary single-peak solutions, boundary multiple-peak solutions, and interior single-peak solutions.

We use a local refinement adaptive finite element method (FEM) to calculate positive solutions of the system (1.1) with finite energy on three different kinds of domain. In our simulations, the parameter $\varepsilon$ can go down to $10^{-4}$. For an elliptic domain with Dirichlet or Neumann boundary conditions, our numerical results are consistent with theoretical results — cf. Refs. [4, 10, 13, 14]. Furthermore, for dumbbell and circular ring domains we

https://doi.org/10.4208/eajam.030616.130517a Published online by Cambridge University Press

report some new phenomena for Dirichlet boundary conditions. We introduce our numerical scheme in Section 2, and in Section 3 discuss our numerical results for the system (1.1) with each of the two different kinds of boundary condition and the different domains Ω. Our conclusions are summarised in Section 4.

## 2. Finite Element Method with Adaptive Grid Refinement

### 2.1. Weak solutions and finite element discretisation

We now consider the numerical solution of the system (1.1) subject to the boundary condition (1.2) or (1.3) for $V = H_0^1(\Omega)$ (or $H^1(\Omega)$), and write $U = (u, v)$. The vector $U = (u, v)$ is called a weak solution if

$$\begin{aligned}
&(\varepsilon^2 \nabla u, \nabla \varphi)_\Omega + (u, \varphi)_\Omega = (\mu_1 u^3 + \beta\, u v^2,\, \varphi)_\Omega\,, \\
&(\varepsilon^2 \nabla v, \nabla \varphi)_\Omega + (v, \varphi)_\Omega = (\mu_1 v^3 + \beta\, v u^2,\, \varphi)_\Omega\,, \\
&\text{for all } \varphi \in V\,,
\end{aligned} \tag{2.1}$$

where $(.,.)_\Omega$ denotes the $L^2$ inner product on Ω. Clearly, any weak solution $U \in V \times V$ is a critical point of the energy functional (1.4). This discrete variational formulation (2.1) is to be solved approximately to produce $(u_h, v_h) \in V_h$ in a finite-dimensional subspace $V_h \subset V$ such that

$$\begin{aligned}
&(\varepsilon^2 \nabla u_h, \nabla \varphi_h)_\Omega + (u_h, \varphi_h)_\Omega = (\mu_1 u_h^3 + \beta\, u_h v_h^2, \varphi_h)_\Omega\,, \\
&(\varepsilon^2 \nabla v_h, \nabla \varphi_h)_\Omega + (v_h, \varphi_h)_\Omega = (\mu_1 v_h^3 + \beta\, v_h u_h^2, \varphi_h)_\Omega\,, \\
&\text{for all } \varphi_h \in V_h\,.
\end{aligned} \tag{2.2}$$

We choose the finite element subspace

$$V_h = \left\{\varphi \in V : \varphi|_C \in P_1(C), C \in \Gamma_h\right\},$$

where $\Gamma_h$ is a decomposition of Ω, $C$ consists of triangles with diameter $h_C$, and $P_1(C)$ is the space of all linear functions on $C$. We choose a nodal basis $\{\phi_h^i, i = 1, \cdots, N\}$ of the finite element space $V_h$ where $dim(V_h) = N$, so the numerical solutions $u_h, v_h$ written in terms of this basis are $u_h = \Sigma_{i=1}^N u_i \phi_h^i$, $v_h = \Sigma_{i=1}^N v_i \phi_h^i$ and the discrete system (2.2) can be converted to a system of nonlinear algebraic equations for the vectors $\mathbf{u} = (u_i)_{i=1}^N$ and $\mathbf{v} = (v_i)_{i=1}^N$ — viz.

$$\mathbf{A}\,\mathbf{U} = \mathbf{F(U)}\,, \tag{2.3}$$

where the matrix $A = \begin{pmatrix} B & 0 \\ 0 & B \end{pmatrix}$ with the entries of the sub-matrix $B = (b_{ij})_{i,j=1}^N$ given by $b_{ij} = (\varepsilon^2 \nabla \phi_h^j, \nabla \phi_h^i)_\Omega + (\phi_h^j, \phi_h^i)_\Omega$, the vector $\mathbf{U} = (\mathbf{u}, \mathbf{v})^T$ (where $T$ denotes the transpose), and the vector on the right hand side corresponding to the nonlinearity is

$$\begin{aligned}
&\mathbf{F(U)} = \left[\mathbf{F}_1(\mathbf{U}); \mathbf{F}_2(\mathbf{U})\right]', \\
&\left(\mathbf{F}_1(\mathbf{U})\right)_i = \left(f_1(u_h, v_h), \phi_h^i\right)_\Omega\,, \\
&\left(\mathbf{F}_2(\mathbf{U})\right)_i = \left(f_2(u_h, v_h), \phi_h^i\right)_\Omega, \quad i = 1, \cdots, N\,,
\end{aligned} \tag{2.4}$$

https://doi.org/10.4208/eajam.030616.130517a Published online by Cambridge University Press

where $f_1(u,v)=\mu_1 u^3+\beta u v^2$, $f_2(u,v)=\mu_2 v^3+\beta v u^2$.

## 2.2. Algorithm and relative descriptions

Now we are ready to provide our finite element method with adaptive grid refinements for finding multiple solutions to the singularly perturbed system (1.1).

**Algorithm 2.1. A finite element method with adaptive grid refinements.**

**Step1.** Generate an initial mesh $\tau_0$ on $\Omega$.

**Step 2.** Set the permissible nonlinear iterative residual $Tol>0$, the refinement number $l=0$, the permissible maximal number of triangles **Maxt**, the permissible maximal number of refinements **Ngen**, and an initial guess $U_0$.

**Step 3.** Set the iteration $j=0$, line search step length $\alpha=1$, and calculate the residual $nr2=\|r_l^{(0)}\|_\infty=\|(AU-F)(U_l)\|_\infty$.

**Step 4.** If $nr2<Tol$, set $U_l=U_l^{(j)}$, go to **Step8**; otherwise, go to **Step5**.

**Step 5.** Compute an approximation Newton descent direction $d$ of $r=AU-F$ at the $U_l^{(j)}$.

**Step 6.** Update $U_l^{(j+1)}=U_l^{(j)}+\alpha d$.

**Step 7.** Calculate the updated residual $nrr=\|r_l^{(j+1)}\|_\infty=\|(AU-F)(U_l^{(j+1)})\|_\infty$. Then if $nr2-nrr<(\alpha/2)nrr$, set $\alpha=\alpha/2$, and go to **Step5**; otherwise, set $nr2=nrr$, $j=j+1$, $\alpha=1$ and go to **Step 4**.

**Step 8.** Calculate error estimates for the adaption ERRF, and choose the triangle selection method to provide the required refined triangles M. If M is not empty, and the existing number of triangles < Maxt and $l<$ Ngen, go to **Step 9**; otherwise, output $U_l$, stop.

**Step 9.** Refine mesh on the required refined triangles $\tau_l\subset\tau_{l+1}$, interpolate $U_l\to U_{l+1}\in\tau_{l+1}$, set $l=l+1$ and go to **Step3**.

**Remark 2.1.** In Step 7, the symbol $\alpha$ defines the Armijo-Goldstein line search step size, which improves the convergence from bad initial guesses by choosing the largest step size from the sequence $1,1/2,1/4,\cdots$ such that

$$\left\|r(U^{(n)})\right\|-\left\|r(U^{(n)}+\alpha p_n)\right\|\geq\frac{\alpha}{2}\left\|r(U^{(n)})\right\|, \tag{2.5}$$

to guarantee a reduction of the residual norm by at least $1-(\alpha/2)$.

**Remark 2.2.** In Step 8, the error estimate ERRF in each triangle $K$ of the mesh includes the residual error and jump error — i.e.

$$\begin{aligned}ERRF_K=&\xi\left(\|\mathscr{R}_u\|_{L^2(K)}+\|\mathscr{R}_v\|_{L^2(K)}\right)\\&+\eta\left(\sqrt{\frac{1}{2}\sum_{e\in\partial K}\varepsilon^2 h_e\|Jmp(u_h)|_e\|^2_{L^2(e)}}+\sqrt{\frac{1}{2}\sum_{e\in\partial K}\varepsilon^2 h_e\|Jmp(v_h)|_e\|^2_{L^2(e)}}\right),\end{aligned}$$

https://doi.org/10.4208/eajam.030616.130517a Published online by Cambridge University Press

Table 1: Asymptotic behaviour of two-spike synchronised solution with both peaks located at the local maximum points of $H(P)(\beta = 0.5)$.

| $\varepsilon$ | $J_\varepsilon(u_h, v_h)$ | $u_{h,max}$ | $v_{h,max}$ | $u_{h,maxpoint}$ | $v_{h,maxpoint}$ |
|---|---|---|---|---|---|
| 2.00e-01 | 1.570e-01 | 1.7470 | 1.0086 | (1.003,-0.030),(-1.003,-0.030) | (1.003,-0.030),(-1.003,-0.030) |
| 1.00e-01 | 5.090e-02 | 1.8747 | 1.0824 | (1.000,0.002),(-1.000,-0.002) | (1.000,0.002),(-1.000,-0.002) |
| 1.00e-02 | 6.526e-04 | 2.0284 | 1.1730 | (1.000,0.001),(-1.000,-0.001) | (1.000,0.001),(-1.000,-0.001) |
| 1.00e-03 | 6.675e-06 | 2.0415 | 1.1807 | (1.000,2.59e-4),(-1.000,-2.59e-4) | (1.000,2.59e-4),(-1.000,-2.59e-4) |
| 1.00e-04 | 6.694e-08 | 2.0450 | 1.1826 | (1.000,1.39e-5),(-1.000,-1.39e-5) | (1.000,1.39e-5),(-1.000,-1.39e-5) |

where $\mathscr{R}_u = u_h - \mu_1 u_h^3 - \beta v_h^2 u_h$, $\mathscr{R}_v = v_h - \mu_2 v_h^3 - \beta u_h^2 v_h$, $Jmp(U_h)|_e$ is the jump of $\nabla U_h$ across $e \in \partial K$, and $\xi$ and $\eta$ are parameters.

## 3. Numerical Results

As previously mentioned, we undertook numerical simulations for three different types of solution domain — viz. elliptic, dumbbell and circular ring. For the elliptic domain, we used both Dirichlet and Neumann boundary conditions. For the dumbbell or circular ring domain, we only considered the Dirichlet boundary condition. Theoretical analysis has shown that the value of $\beta$ decides the solution branches [4, 10, 13, 14]. In our numerical simulations, we adopted the fixed parameter values $\mu_1 = 1$ and $\mu_2 = 2$, and varied the parameter $\beta \geq 0$ —- and in general, when $0 \leq \beta < 1$ or $\beta > 2$ we found solution branches.

### 3.1. Elliptic domain

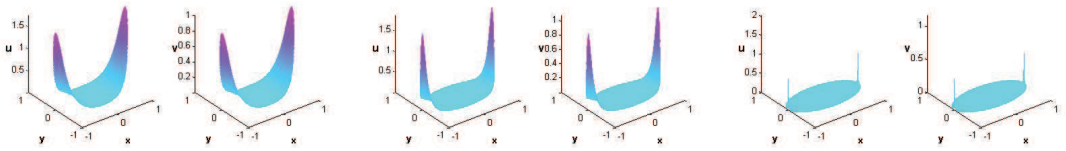
For the elliptic domain $\Omega = \{(x, y) | x^2 + 4y^2 < 1\}$, we set the permissible residual $tol$ at $\varepsilon \times 10^{-8}$. According to the definition of $H(P)$ and $dist(P, \partial\Omega)$, we know that $H(P)$ has two local maximum points located at $(1, 0)$ and $(-1, 0)$, and also two local minimum points located at $(0, 0.5)$ and $(0, -0.5)$, while $dist(P, \partial\Omega)$ has only one local maximum point located at $(0, 0)$. Under either homogeneous Dirichlet or Neumann boundary conditions, we chose reasonable initial data and obtained the following results.

#### 3.1.1. Homogeneous Neumann boundary condition

(I) Choosing $\beta = 0.5$ and the initial data $u_0 = v_0 = 0.75\cos(1 - x^2 - 4y^2)$, we obtained positive solutions for the system (1.1) and the asymptotic behaviour evident in Table 1. When $\beta = 0.5$, there is a positive synchronised numerical solution $(u_h, v_h)$, where both $u_h$ and $v_h$ have two spikes — cf. Fig. 1. We see that the peaks of $u_h$ and $v_h$ become sharper and narrower as $\varepsilon$ decreases. Secondly, we set $\varepsilon = 0.1$ and adopted the values $\beta = 0.999, 2.001$ and 2.5, producing the solutions shown in Fig. 2 for the same initial data $u_0 = v_0 = 0.75\cos(1 - x^2 - 4y^2)$.

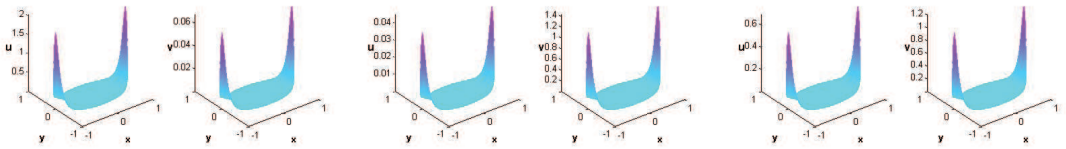
(II) Choosing the initial data $u_0 = v_0 = 0.5\cos(1 - x^2 - 4y^2) - 2(1 - x^2 - 4y^2)^2 x^2$, for $\beta = 0.5$ and 2.5 we obtained positive solutions for the system (1.1) as shown in Fig. 3 and Table 2. There is a positive synchronised numerical solution $(u_h, v_h)$, where $u_h$ and $v_h$ both

https://doi.org/10.4208/eajam.030616.130517a Published online by Cambridge University Press



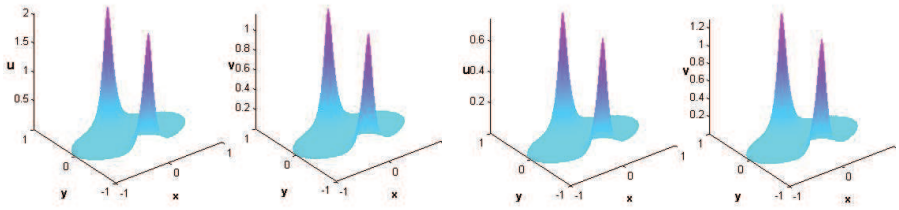
(a) $\varepsilon = 0.2$ (b) $\varepsilon = 10^{-1}$ (c) $\varepsilon = 10^{-2}$

Figure 1: Two-spike synchronised solution with both peaks at the local maximum points of $H(P)$, (a)-(c) show the solution $(u_h, v_h)$ for various $\varepsilon$, where the left side in each figure shows $u_h$ and the right side $v_h$.



(a) $\beta = 0.999$ (b) $\beta = 2.001$ (c) $\beta = 2.5$

Figure 2: Two-spike synchronised solution with both peaks at the local maximum points of $H(P)$, (a)-(c) show the solution $(u_h, v_h)$ for various $\beta$, where the left side in each figure shows $u_h$ and the right side $v_h$.



(a) $\beta = 0.5$ (b) $\beta = 2.5$

Figure 3: Two-spike synchronised solution with both peaks at the local minimum points of $H(P)$, (a), (b) show the solution $(u_h, v_h)$ when $\varepsilon = 0.1$ for $\beta = 0.5$ and 2.5, where the left side in each figure shows $u_h$ and the right side $v_h$.

have two spikes that behave synchronously. As $\varepsilon \to 0$, the maximum values of $u_h$ and $v_h$ tend to constants, while the location of one peak tends to (0,0.5) and the other to $(0,-0.5)$.

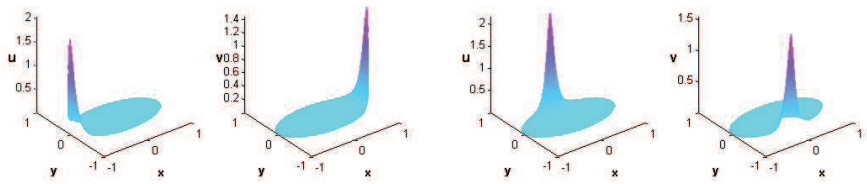
(III) Choosing $\beta = 0.5$ and various initial data, we obtained two different types of positive solution for the system (1.1). These two types of positive segregated numerical solution $(u_h, v_h)$ are shown in Table 3 and Fig. 4. Both $u_h$ and $v_h$ have only one spike, and as $\varepsilon$ decreases the peaks of $u_h$ becomes sharper and narrower. When $\varepsilon \to 0$, the location of the peak of $u_h$ tends to $(-1,0)$ and the peak of $v_h$ to $(1,0)$, and the peak of $u_h$ tends to $(0,0.5)$ and the peak of $v_h$ to $(0,-0.5)$, respectively.

(IV) Choosing the initial data $u_0 = v_0 = 0.5\cos(1-x^2-4y^2)-2(1-x^2-4y^2)^2(x+0.2)^2$, we obtained a positive least energy solution of the system (1.1) for $\beta = 0.5$ and 2.5 as shown in Fig. 5. The asymptotic behaviour is evident in Table 4, showing the positive synchronised numerical solution $(u_h, v_h)$. Both $u_h$ and $v_h$ have only one spike and are synchronous, and as $\varepsilon$ decreases the peak of $u_h$ and $v_h$ becomes sharper and narrower. When $\varepsilon \to 0$, the peak of both $u_h$ and $v_h$ tends to $(-1,0)$.

https://doi.org/10.4208/eajam.030616.130517a Published online by Cambridge University Press

Table 2: Asymptotic behaviour of the two-spike synchronised solution with both peaks at the local minimum points of $H(P)$ ($\beta = 0.5$ and 2.5).

| $\beta$ | $\varepsilon$ | $J_\varepsilon(u_h, v_h)$ | $u_{h,max}$ | $v_{h,max}$ | $u_{h,maxpoint}$ | $v_{h,maxpoint}$ |
|---|---|---|---|---|---|---|
| 0.5 | 2.00e-01 | 2.278e-01 | 1.9291 | 1.1138 | (6.12e-17,0.50),(-0.001,-0.498) | (6.123e-17,0.500),(-0.001,-0.498) |
| | 1.00e-01 | 6.480e-02 | 2.0226 | 1.1684 | (-0.008,0.500),(-6.17e-3,-0.500) | (-0.008,0.500),(-6.17e-3,-0.500) |
| | 1.00e-02 | 6.669e-04 | 2.0413 | 1.1793 | (-0.002,0.500),(5.91e-4,-0.500) | (-0.002,0.500),(5.91e-4,-0.500) |
| | 1.00e-03 | 6.689e-06 | 2.0424 | 1.1799 | (3.53e-4,0.500),(9.06e-5,-0.500) | (3.53e-4,0.500),(9.06e-5,-0.500) |
| | 1.00e-04 | 6.690e-08 | 2.0433 | 1.1804 | (-9.24e-6,0.500),(-4.62e-5,-0.500) | (-9.24e-6,0.500),(-4.62e-5,-0.500) |
| 2.5 | 2.00e-01 | 9.380e-01 | 0.7147 | 1.2379 | (6.12e-17,0.50),(-0.001,-0.498) | (6.123e-17,0.500),(-0.001,-0.498) |
| | 1.00e-01 | 2.670e-02 | 0.7488 | 1.2999 | (-0.008,0.500),(-2.40e-3,-0.500) | (-0.008,0.500),(-2.40e-3,-0.500) |
| | 1.00e-02 | 2.749e-04 | 0.7558 | 1.3120 | (-0.002,0.500),(5.91e-4,-0.500) | (-0.002,0.500),(5.91e-4,-0.500) |
| | 1.00e-03 | 2.755e-06 | 0.7562 | 1.3127 | (3.53e-4,0.500),(9.06e-5,-0.500) | (3.53e-4,0.500),(9.06e-5,-0.500) |
| | 1.00e-04 | 2.757e-08 | 0.7564 | 1.3131 | (-9.24e-6,0.500),(-4.62e-5,-0.500) | (-9.24e-6,0.500),(-4.62e-5,-0.500) |



(a) (b)

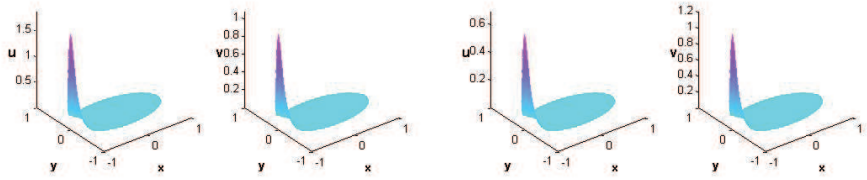
Figure 4: One-spike segregated solution, (a),(b) show the solution $(u_h, v_h)$ when $\varepsilon = 0.1$ for the initial data $u_0 = 0.5\cos(1-x^2-4y^2)-2(1-x^2-4y^2)^2(x+0.2)^2$, $v_0 = 0.5\cos(1-x^2-4y^2)-2(1-x^2-4y^2)^2(x-0.2)^2$ and $u_0 = 0.5\cos(1-x^2-4y^2)-2(1-x^2-4y^2)^2(y-0.2)^2$, $v_0 = 0.5\cos(1-x^2-4y^2)-2(1-x^2-4y^2)^2(y+0.2)^2$, respectively. The left side in each figure shows $u_h$ and the right side $v_h$.

Table 3: Asymptotic behaviour of the one-spike segregated solution ($\beta = 0.5$).

| $\varepsilon$ | $J_\varepsilon(u_h, v_h)$ | $u_{h,max}$ | $v_{h,max}$ | $u_{h,maxpoint}$ | $v_{h,maxpoint}$ |
|---|---|---|---|---|---|
| 2.00e-01 | 1.032e-01 | 1.8878 | 1.3348 | (-1.0003,-6.1232e-17) | (1.0003,6.1232e-17) |
| 1.00e-01 | 3.380e-02 | 2.0472 | 1.4509 | (-0.9991,0.0213) | (0.9972,-0.0377) |
| 1.00e-02 | 4.282e-04 | 2.1858 | 1.5521 | (-1.0000,5.9128e-4) | (1.0000,2.9564e-4) |
| 1.00e-03 | 4.380e-06 | 2.2057 | 1.5596 | (-1.0000,2.5912e-5) | (1.0000,2.5912e-5) |
| 2.00e-01 | 1.638e-01 | 2.1599 | 1.5250 | (-0.0568,0.4992) | (0.047,-0.5000) |
| 1.00e-01 | 4.260e-02 | 2.1865 | 1.5459 | (-0.0355,0.4997) | (-0.0378,-0.4996) |
| 1.00e-02 | 4.376e-04 | 2.2046 | 1.5588 | (-0.0011,0.5000) | (-0.0058,-0.5000) |
| 1.00e-03 | 4.389e-06 | 2.2093 | 1.5596 | (1.8480e-5,0.5000) | (2.5872e-4,-0.5000) |

(V) For the initial data $u_0 = v_0 = (1-x^2-4y^2)^2$, we obtained a positive interior solution of the system (1.1) for $\beta = 0.5$ and 2.5 — cf. Fig. 6. The asymptotic behaviour is evident in Table 5, which shows the positive numerical solution $(u_h, v_h)$ where $u_h$ and $v_h$ both have only one spike and are synchronous. As $\varepsilon$ decreases, the peak of $u_h$ and $v_h$ becomes sharper and narrower. When $\varepsilon \to 0$, the location of the peak of $u_h$ and $v_h$ tends to (0,0).

https://doi.org/10.4208/eajam.030616.130517a Published online by Cambridge University Press

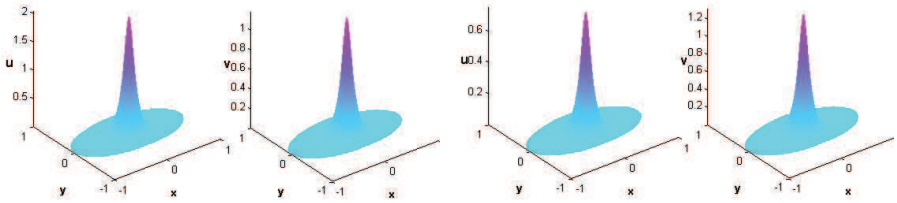


(a) $\beta = 0.5$ (b) $\beta = 2.5$

Figure 5: One-spike synchronous solution with the peak at local maximum of $H(P)$, (a)(b) show the solution $(u_h, v_h)$ for various $\beta$ when $\varepsilon = 0.1$. The left side in each figure shows $u_h$ and the right side $v_h$.

Table 4: Asymptotic behaviour of synchronous solution with one peak at local maximum of $H(P)$.

| $\beta$ | $\varepsilon$ | $J_\varepsilon(u_h, v_h)$ | $u_{h,max}$ | $v_{h,max}$ | $u_{h,maxpoint}$ | $v_{h,maxpoint}$ |
|---|---|---|---|---|---|---|
| 0.5 | 2.00e-01 | 7.860e-02 | 1.7474 | 1.0089 | (-1.0003,-6.1232e-17) | (-1.0003,-6.1232e-17) |
| | 1.00e-01 | 2.540e-02 | 1.8747 | 1.0823 | (-0.9991,0.0213) | (-0.9991,0.0213) |
| | 1.00e-02 | 3.263e-04 | 2.0270 | 1.1710 | (-1.0000,5.9128e-4) | (-1.0000,5.9128e-4) |
| | 1.00e-03 | 3.335e-06 | 2.0381 | 1.1774 | (-1.0000,2.5912e-5) | (-1.0000,2.5912e-5) |
| | 1.00e-04 | 3.345e-08 | 2.0424 | 1.1799 | (-1.0000,-2.3097e-6) | (-1.0000,-2.3097e-6) |
| 2.5 | 2.00e-01 | 3.240e-02 | 0.6474 | 1.1213 | (-1.0003,-6.1232e-17) | (-1.0003,-6.1232e-17) |
| | 1.00e-01 | 1.050e-02 | 0.6945 | 1.2030 | (-0.9991,0.0213) | (-0.9991,0.0213) |
| | 1.00e-02 | 1.344e-04 | 0.7510 | 1.3008 | (-1.0000,5.9128e-4) | (-1.0000,5.9128e-4) |
| | 1.00e-03 | 1.374e-06 | 0.7563 | 1.3084 | (-1.0000,2.5912e-5) | (-1.0000,2.5912e-5) |
| | 1.00e-04 | 1.378e-08 | 0.7578 | 1.3111 | (-1.0000,-2.3097e-6) | (-1.0000,-2.3097e-6) |



(a) $\beta = 0.5$ (b) $\beta = 2.5$

Figure 6: Interior spike synchronised solution with the peak located at a local maximum point of $dist(P, \partial\Omega)$, (a),(b) show the solution $(u_h, v_h)$ for various $\beta$ when $\varepsilon = 0.1$, where the left side in each figure shows $u_h$ and the right side $v_h$.

### 3.1.2. Homogeneous Dirichlet boundary condition

We considered $\Omega_1 = \{(x, y) | x^2 + 4y^2 < r^2\}$ and $\Omega_2 = \Omega \backslash \Omega_1$, $r \in [0.05, 0.5]$.

(VI) For $\beta = 0.5$ and the initial data

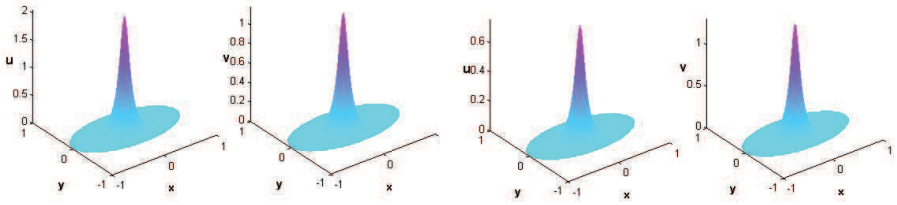
$$u_0 = v_0 = \begin{cases} \frac{1}{r^2}(r^2 - x^2 - 4y^2), & (x, y) \in \Omega_1 \\ 0, & (x, y) \in \Omega_2 \end{cases},$$

we obtained a least energy solution of the system (1.1) when $\beta = 0.5$ and 2.5 as shown in Fig. 7. The asymptotic behaviour is evident in Table 6 when $\beta = 0.5$ and $\beta = 2.5$ for a positive numerical solution $(u_h, v_h)$. Both $u_h$ and $v_h$ have only one spike and are

https://doi.org/10.4208/eajam.030616.130517a Published online by Cambridge University Press

Table 5: Asymptotic behaviour of the interior spike synchronised solution with the peak located at a local maximum point of $dist(P, \partial\Omega)$.

| $\beta$ | $\varepsilon$ | $J_\varepsilon(u_h, v_h)$ | $u_{h,max}$ | $v_{h,max}$ | $u_{h,maxpoint}$ | $v_{h,maxpoint}$ |
|---|---|---|---|---|---|---|
| 0.5 | 2.00e-01 | 2.394e-01 | 1.9558 | 1.1292 | (1.7919e-4,-0.0011) | (1.7919e-4,-0.0011) |
| | 1.00e-01 | 6.680e-02 | 2.0420 | 1.1809 | (0.0394,0.0070) | (0.0394,0.0070) |
| | 1.00e-02 | 6.691e-04 | 2.0423 | 1.1811 | (0.0033,-0.0015) | (0.0033,-0.0015) |
| | 1.00e-03 | 6.694e-06 | 2.0427 | 1.1813 | (-7.2068e-5,7.5849e-5) | (-7.2068e-5,7.5849e-5) |
| | 1.00e-04 | 6.693e-08 | 2.0427 | 1.1813 | (-3.1647e-5,1.0836e-5) | (-3.1647e-5,1.0836e-5) |
| 2.5 | 2.00e-01 | 9.860e-02 | 0.7246 | 1.2550 | (1.7919e-4,-0.0011) | (1.7919e-4,-0.0011) |
| | 1.00e-01 | 2.750e-02 | 0.7567 | 1.3107 | (0.0393,0.0058) | (0.0393,0.0058) |
| | 1.00e-02 | 2.756e-04 | 0.7579 | 1.3113 | (0.0033,-0.0015) | (0.0033,-0.0015) |
| | 1.00e-03 | 2.757e-06 | 0.7581 | 1.3115 | (-7.2068e-5,7.5849e-5) | (-7.2068e-5,7.5849e-5) |
| | 1.00e-04 | 2.757e-08 | 0.7581 | 1.3115 | (-3.1647e-5,1.0836e-5) | (-3.1647e-5,1.0836e-5) |



(a) $\beta = 0.5$ (b) $\beta = 2.5$

Figure 7: Least energy solution with the peak located at a local maximum point of $dist(P, \partial\Omega)$, (a),(b) show the solution $(u, v)$ for various $\beta$ when $\varepsilon = 0.1$, where the left side in each figure shows $u$ and the right side $v$.

Table 6: Asymptotic behaviour of the least energy solution with the peak at a local maximum point of $dist(P, \partial\Omega)$.

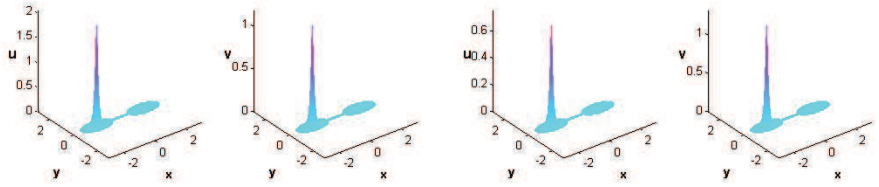
| $\beta$ | $\varepsilon$ | $J_\varepsilon(u_h, v_h)$ | $u_{h,max}$ | $v_{h,max}$ | $u_{h,maxpoint}$ | $v_{h,maxpoint}$ |
|---|---|---|---|---|---|---|
| 0.5 | 5.00e-01 | 4.248e+00 | 3.1395 | 1.8162 | (1.7919e-4,-0.0011) | (1.7919e-4,-0.0011) |
| | 1.00e-01 | 6.690e-02 | 2.0428 | 1.1815 | (-2.8826e-4,0.0059) | ((-2.8826e-4,0.0059) |
| | 1.00e-02 | 6.689e-04 | 2.0426 | 1.1813 | (0.0012,-0.0021) | (0.0012,-0.0021) |
| | 1.00e-03 | 6.693e-06 | 2.0425 | 1.1812 | (4.2746e-5,-6.6814e-5) | (4.2746e-5,-6.6814e-5) |
| | 1.00e-04 | 6.690e-08 | 2.0425 | 1.1812 | (7.7131e-6,8.7340e-6) | (7.7131e-6,8.7340e-6) |
| 2.5 | 5.00e-01 | 1.749e+00 | 1.1631 | 2.0146 | (1.7919e-4,-0.0011) | (1.7919e-4,-0.0011) |
| | 1.00e-01 | 2.760e-02 | 0.7581 | 1.3115 | (-2.8826e-4,0.0059) | ((-2.8826e-4,0.0059) |
| | 1.00e-02 | 2.756e-04 | 0.7579 | 1.3113 | (0.0012,-0.0021) | (0.0012,-0.0021) |
| | 1.00e-03 | 2.757e-06 | 0.7569 | 1.3110 | (4.2746e-5,-6.6814e-5) | (4.2746e-5,-6.6814e-5) |
| | 1.00e-04 | 2.754e-08 | 0.7568 | 1.3109 | (7.7131e-6,8.7340e-6) | (7.7131e-6,8.7340e-6) |

synchronous, and as $\varepsilon$ decreases the peak of $u_h$ and $v_h$ becomes sharper and narrower. When $\varepsilon \to 0$, the location of the peak of $u_h$ and $v_h$ tends to (0,0).

## 3.2. Dumbbell domain

We set $\Omega_3 = \{(x, y)|(x + 1.5)^2 + 4y^2 < 1\}$, $\Omega_4 = \{(x, y)|(x - 1.5)^2 + 4y^2 < 1\}$, $\Omega_5 = \{(x, y)| - 0.6 < x < 0.6, -0.1 < y < 0.1\}$ with $\Omega = \Omega_3 \cup \Omega_4 \cup \Omega_5$, and also took

https://doi.org/10.4208/eajam.030616.130517a Published online by Cambridge University Press



(a) $\beta = 0.5$ (b) $\beta = 2.5$

Figure 8: One-spike synchronised solution with the peak located one local maximum point of $dist(P, \partial\Omega)$, (a),(b) show the solution $(u_h, v_h)$ for $\beta = 0.5$ and $\beta = 2.5$ when $\varepsilon = 0.1$, where the left side in each figure shows $u_h$ and the right side $v_h$.

Table 7: Asymptotic behaviour of One-spike synchronised solution with the peak located at one local maximum point of $dist(P, \partial\Omega)$.

| $\beta$ | $\varepsilon$ | $J_\varepsilon(u_h, v_h)$ | $u_{h,max}$ | $v_{h,max}$ | $u_{h,maxpoint}$ | $v_{h,maxpoint}$ |
|---|---|---|---|---|---|---|
| 0.5 | 5.00e-01 | 4.249e+00 | 3.1402 | 1.8130 | (-1.502,0.001) | (-1.502,0.001) |
| | 1.00e-01 | 6.690e-02 | 2.0429 | 1.1802 | (-1.505,-0.001) | (-1.505,-0.001) |
| | 1.00e-02 | 6.688e-04 | 2.0425 | 1.1800 | (-1.499,0.000) | (-1.499,0.000) |
| | 1.00e-03 | 6.689e-06 | 2.0427 | 1.1801 | (-1.500,0.000) | (-1.500,0.000) |
| | 1.00e-04 | 6.688e-08 | 2.0425 | 1.1800 | (-1.500,0.000) | (-1.500,0.000) |
| 2.5 | 5.00e-01 | 1.750e+00 | 1.1634 | 2.0150 | (-1.502,0.001) | (-1.502,0.001) |
| | 1.00e-01 | 2.760e-02 | 0.7570 | 1.3112 | (-1.505,-0.001) | (-1.505,-0.001) |
| | 1.00e-02 | 2.754e-04 | 0.7568 | 1.3108 | (-1.499,0.000) | (-1.499,0.000) |
| | 1.00e-03 | 2.754e-06 | 0.7568 | 1.3109 | (-1.500,0.000) | (-1.500,0.000) |
| | 1.00e-04 | 2.754e-08 | 0.7568 | 1.3108 | (-1.500,0.000) | (-1.500,0.000) |

$\Omega_6 = \{(x,y)|(x+1.5)^2+4y^2 \le r^2\}$, $\Omega_7 = \{(x,y)|(x-1.5)^2+4y^2 \le r^2\}$, $r \in [0.05, 0.5]$, and the permissible residual $tol = \varepsilon \times 10^{-8}$. We know that $dist(P, \partial\Omega)$ has two local maximum points located at $(-1.5, 0)$ and $(1.5, 0)$. For the homogeneous Dirichlet boundary condition, we chose some reasonable initial data to obtain our results.

(VII) For the initial data

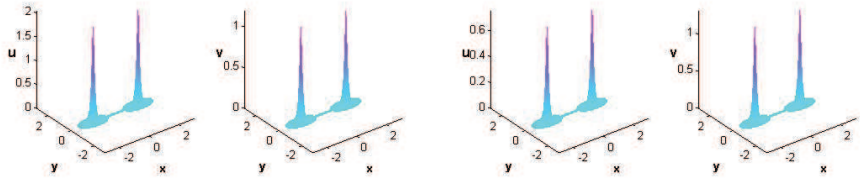
$$u_0 = v_0 = \begin{cases} \frac{1}{r^2}(r^2 - (x+1.5)^2 - 4y^2), & (x,y) \in \Omega_6, \\ 0\,, & (x,y) \in \Omega \backslash \Omega_6, \end{cases}$$

we obtained a least energy solution as shown in Fig. 8. The asymptotic behaviour is evident in Table 7. When $\beta = 0.5$ and $\beta = 2.5$, there is a positive synchronised numerical solution $(u_h, v_h)$. Both $u_h$ and $v_h$ have only one spike and are synchronous. As $\varepsilon$ decreases, the peak of $u_h$ and $v_h$ becomes sharper and narrower. When $\varepsilon \to 0$, the location of the peak of $u_h$ and $v_h$ tends to $(-1.5, 0)$.

(VIII) Choosing the initial data

$$u_0 = v_0 = \begin{cases} \frac{1}{r^2}(r^2 - (x+1.5)^2 - 4y^2), & (x,y) \in \Omega_6 \\ \frac{1}{r^2}(r^2 - (x-1.5)^2 - 4y^2), & (x,y) \in \Omega_7 \\ 0\,, & (x,y) \in \Omega \backslash (\Omega_6 \bigcup \Omega_7) \end{cases},$$

https://doi.org/10.4208/eajam.030616.130517a Published online by Cambridge University Press



(a) $\beta = 0.5$ (b) $\beta = 2.5$

Figure 9: Two-spike synchronised solutions with peaks located at local maximum points of $dist(P, \partial\Omega)$, (a),(b) show the solution $(u_h, v_h)$ for $\beta = 0.5$ and $\beta = 2.5$ when $\varepsilon = 0.1$, where the left side in each figure shows $u_h$ and the right side $v_h$.

Table 8: The asymptotic behaviour of two-spike synchronised solution with peaks located at local maximum points of $dist(P, \partial\Omega)$.

| $\beta$ | $\varepsilon$ | $J_\varepsilon(u_h, v_h)$ | $u_{h,max}$ | $v_{h,max}$ | $u_{h,maxpoint}$ | $v_{h,maxpoint}$ |
|---|---|---|---|---|---|---|
| 0.5 | 5.00e-01 | 8.498e+00 | 3.3918 | 2.3984 | (-1.502,0.001),(1.501,-0.002) | (-1.502,0.001),(1.501,-0.002) |
| | 1.00e-01 | 1.341e-01 | 2.0469 | 1.1967 | (-1.505,-0.001), (1.499,-0.017) | (-1.505,-0.001),(1.499,-0.017) |
| | 1.00e-02 | 1.300e-03 | 2.0428 | 1.1800 | (-1.499,0.000),(1.498,-0.001) | (-1.499,0.000),(1.498,-0.001) |
| | 1.00e-03 | 1.338e-05 | 2.0427 | 1.1801 | (-1.500,0.000),(1.500,0.001) | (-1.500,0.000),(1.500,0.001) |
| | 1.00e-04 | 1.338e-07 | 2.0427 | 1.1800 | (-1.500,0.000),(1.500,0.000) | (-1.500,0.000),(1.500,0.000) |
| 2.5 | 5.00e-01 | 3.499e+00 | 1.1633 | 2.0150 | (-1.502,0.001),(1.501,-0.002) | (-1.502,0.001),(1.501,-0.002) |
| | 1.00e-01 | 5.520e-02 | 0.7584 | 1.3132 | (-1.505,-0.001), (1.499,-0.017) | (-1.505,-0.001),(1.499,-0.017) |
| | 1.00e-02 | 5.508e-04 | 0.7568 | 1.3108 | (-1.499,0.000),(1.498,-0.001) | (-1.499,0.000),(1.498,-0.001) |
| | 1.00e-03 | 5.508e-06 | 0.7568 | 1.3109 | (-1.500,0.000),(1.500,0.001) | (-1.500,0.000),(1.500,0.001) |
| | 1.00e-04 | 5.507e-08 | 0.7568 | 1.3108 | (-1.500,0.000),(1.500,0.000) | (-1.500,0.000),(1.500,0.000) |

we obtained a two-spike solution as shown in Fig. 9. The asymptotic behaviour is evident in Table 8. When $\beta = 0.5$ and $\beta = 2.5$, there is a positive synchronised numerical solution. Both $u_h$ and $v_h$ have two spikes and are synchronous, and as $\varepsilon$ decreases the peaks of $u_h$ and $v_h$ becomes sharper and narrower. When $\varepsilon \to 0$, the location of one peak of $u_h$ and $v_h$ tends to $(-1.5, 0)$ and the other to $(1.5, 0)$.

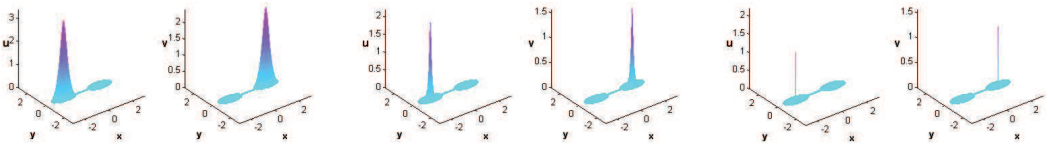
(IX) Choosing $\beta = 0.5$ and the initial data

$$u_0 = \begin{cases} \frac{1}{r^2}(r^2 - (x+1.5)^2 - 4y^2), & (x,y) \in \Omega_6 \\ 0\,, & (x,y) \in \Omega \backslash \Omega_6 \end{cases},$$

$$v_0 = \begin{cases} \frac{1}{r^2}(r^2 - (x-1.5)^2 - 4y^2), & (x,y) \in \Omega_7 \\ 0\,, & (x,y) \in \Omega \backslash \Omega_7 \end{cases},$$

we obtained a segregated solution as shown in Fig. 10 and Table 9. Both $u_h$ and $v_h$ have only one spike and are segregated, and as $\varepsilon$ decreases the peak of $u_h$ and $v_h$ becomes sharper and narrower. When $\varepsilon \to 0$, the location of the peak of $u_h$ tends to $(-1.5, 0)$ and the location of the peak of $v_h$ tends to $(1.5, 0)$.

https://doi.org/10.4208/eajam.030616.130517a Published online by Cambridge University Press

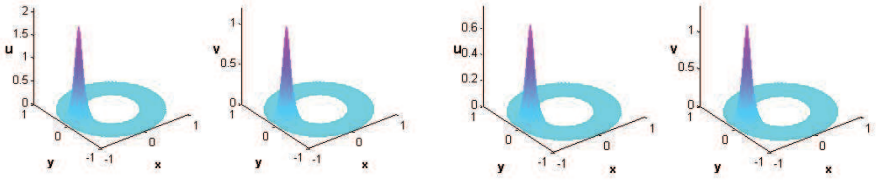


(a) $\varepsilon = 0.5$ (b) $\varepsilon = 10^{-1}$ (c) $\varepsilon = 10^{-2}$

Figure 10: One spike segregated solution with the peak located at one local maximum point of $dist(P, \partial\Omega)$, (a)-(c) show the solution $(u, v)$ for various $\varepsilon$, where the left side in each figure shows $u$ and the right side $v$.

Table 9: Asymptotic behaviour of one spike segregated solution with the peak located at one local maximum point of $dist(P, \partial\Omega)(\beta = 0.5)$.

| $\varepsilon$ | $J_\varepsilon(u_h, v_h)$ | $u_{h,max}$ | $v_{h,max}$ | $u_{h,maxpoint}$ | $v_{h,maxpoint}$ |
|---|---|---|---|---|---|
| 5.00e-01 | 5.577e+00 | 3.3918 | 2.3984 | (-1.502,0.001) | (1.501,-0.002) |
| 1.00e-01 | 8.790e-02 | 2.2073 | 1.5611 | (-1.505,-0.001) | (1.499,-0.017) |
| 1.00e-02 | 8.778e-04 | 2.2063 | 1.5601 | (-1.499,0.000) | (1.498,-0.001) |
| 1.00e-03 | 8.778e-06 | 2.2068 | 1.5601 | (-1.500,0.000) | (1.500,0.001) |
| 1.00e-04 | 8.777e-08 | 2.2063 | 1.5601 | (-1.500,0.000) | (1.500,0.000) |



(a) $\beta = 0.5$ (b) $\beta = 2.5$

Figure 11: One-spike synchronised solution with one peak located at local maximum point of $dist(P, \partial\Omega)$, (a),(b) show the solution $(u_h, v_h)$ for various $\beta$ when $\varepsilon = 0.1$, where the left side in each figure shows $u_h$ and the right side $v_h$.

### 3.3. Circular ring domain

We set $\Omega_8 = \{(x, y)|x^2 + y^2 < 1\}$, $\Omega_9 = \{(x, y)|x^2 + y^2 < 0.25\}$, $\Omega = \Omega_8 \backslash \Omega_9$ and the permissible residual $tol = \varepsilon \times 10^{-8}$ for the circular ring domain. We know that $dist(P, \partial\Omega)$ has an infinite local maximum point located on the circle $\{(x, y)|x^2 + y^2 = 0.75^2\}$. For the homogeneous Dirichlet boundary condition, we chose some reasonable initial data to obtain our results.

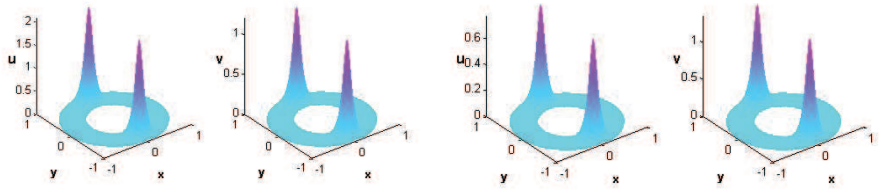
(X) Choosing the iterative initial data $u_0 = 0.3|1 - x|$, $v_0 = 0.18|1 - x|$, we obtained a least-energy solution of the system (1.1) as shown in Fig. 11. The asymptotic behaviour is evident in Table 10. There is a positive synchronised numerical solution $(u_h, v_h)$. Both $u_h$ and $v_h$ have only one spike and are synchronous. As $\varepsilon$ decreases, the peak of $u_h$ and $v_h$ becomes sharper and narrower. When $\varepsilon \to 0$, the location of the peak of $u_h$ and $v_h$ tends to $(-0.75, 0)$.

(XI) For the initial data $u_0 = 1.5(1 - x^2 - 4y^2)$, $v_0 = 1 - x^2 - 4y^2$ we obtained a two-

https://doi.org/10.4208/eajam.030616.130517a Published online by Cambridge University Press

Table 10: Asymptotic behaviour of the one-spike synchronised solution with a peak located at local maximum point of $dist(P,\partial\Omega)$.

| $\beta$ | $\varepsilon$ | $J_\varepsilon(u_h,v_h)$ | $u_{h,max}$ | $v_{h,max}$ | $u_{h,maxpoint}$ | $v_{h,maxpoint}$ |
|---|---|---|---|---|---|---|
| 0.5 | 5.00e-01 | 1.228e+01 | 5.2591 | 3.0363 | (-0.742,0.002) | (-0.742,0.002) |
| | 1.00e-01 | 7.150e-02 | 2.0941 | 1.2091 | (-0.745,-0.010) | (-0.745,-0.010) |
| | 1.00e-02 | 6.685e-04 | 2.0400 | 1.1778 | (-0.748,0.010) | (-0.748,0.010) |
| | 1.00e-03 | 6.688e-06 | 2.0427 | 1.1794 | (-0.750,0.000) | (-0.750,0.000) |
| | 1.00e-04 | 6.686e-08 | 2.0439 | 1.1801 | (-0.750,0.000) | (-0.750,0.000) |
| 2.5 | 5.00e-01 | 5.057e+00 | 1.9484 | 3.3747 | (-0.742,0.002) | (-0.742,0.002) |
| | 1.00e-01 | 2.940e-02 | 0.7758 | 1.3438 | (-0.745,-0.010) | (-0.745,-0.010) |
| | 1.00e-02 | 2.753e-04 | 0.7561 | 1.3095 | (-0.748,0.010) | (-0.748,0.010) |
| | 1.00e-03 | 2.758e-06 | 0.7568 | 1.3109 | (-0.750,0.000) | (-0.750,0.000) |
| | 1.00e-04 | 2.753e-08 | 0.7570 | 1.3112 | (-0.750,0.000) | (-0.750,0.000) |



(a) $\beta = 0.5$ (b) $\beta = 2.5$

Figure 12: Two-spike synchronised solutions with peaks located at two local maximum points of $dist(P,\partial\Omega)$. (a),(b) show the solution $(u_h,v_h)$ under different $\beta$ when $\varepsilon = 0.1$, where the left side in each figure shows $u_h$ and the right side $v_h$.

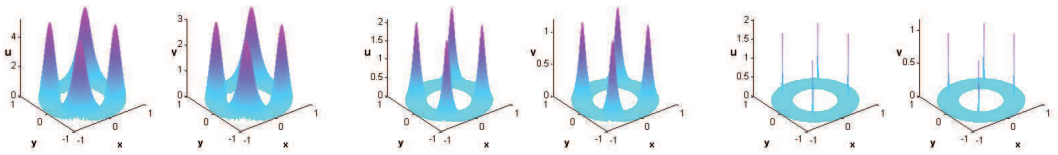
Table 11: The asymptotic behaviour of two-spike synchronised solution with peaks located at two local maximum points of $dist(P,\partial\Omega)$.

| $\beta$ | $\varepsilon$ | $J_\varepsilon(u_h,v_h)$ | $u_{h,max}$ | $v_{h,max}$ | $u_{h,maxpoint}$ | $v_{h,maxpoint}$ |
|---|---|---|---|---|---|---|
| 0.5 | 5.00e-01 | 2.456e+01 | 5.2591 | 3.0363 | (-0.009,-0.741),(0.009,0.741) | (-0.009,-0.741), (0.009,0.741) |
| | 1.00e-01 | 1.429e-01 | 2.0944 | 1.2092 | (-0.004,-0.745),(0.004,0.745) | (-0.004,-0.745), (0.004,0.745) |
| | 1.00e-02 | 1.300e-03 | 2.0437 | 1.1799 | (-0.002,-0.748),(0.002,0.758) | (-0.002,-0.748),(0.002,0.758) |
| | 1.00e-03 | 1.338e-05 | 2.0437 | 1.1797 | (0.000,-0.750),(0.000,0.750) | (0.000,-0.750),(0.000,0.750) |
| 2.5 | 5.00e-01 | 1.011e+01 | 1.9484 | 3.3746 | (-0.009,-0.741),(0.009,0.741) | (-0.009,-0.741), (0.009,0.741) |
| | 1.00e-01 | 5.890e-02 | 0.7759 | 1.3439 | (-0.004,-0.745),(0.004,0.745) | (-0.004,-0.745), (0.004,0.745) |
| | 1.00e-02 | 5.517e-04 | 0.7566 | 1.3135 | (-0.002,-0.748),(0.002,0.758) | (-0.002,-0.748),(0.002,0.758) |
| | 1.00e-03 | 1.338e-05 | 0.7566 | 1.3110 | (0.000,-0.750),(0.000,0.750) | (0.000,-0.750),(0.000,0.750) |

spike solution as shown in Fig. 12. The asymptotic behaviour is evident in Table 11. There is a positive synchronised numerical solution $(u_h,v_h)$. Both $u_h$ and $v_h$ have two spikes and are synchronous. As $\varepsilon$ decreases, the peaks of $u_h$ and $v_h$ becomes sharper and narrower. When $\varepsilon \to 0$, the location of one peak of $u_h$ and $v_h$ tends to $(0,-0.75)$ and the other to $(0,0.75)$.

(XII) Choosing $\beta = 0.5$ and the initial data $u_0 = 4|1-x|$, $v_0 = 1.5|1-x|$, we obtained a four-spike solution as shown in Fig. 13. From the figure, when $\beta = 0.5$, there is a positive synchronised numerical solution $(u_h,v_h)$. Both $u_h$ and $v_h$ have four spikes and are syn-

https://doi.org/10.4208/eajam.030616.130517a Published online by Cambridge University Press



(a) $\varepsilon = 0.5$ (b) $\varepsilon = 10^{-1}$ (c) $\varepsilon = 10^{-2}$

Figure 13: Four-spike synchronised solution with peaks located at local maximum points of $dist(P, \partial\Omega)$. (a)-(c) show the solution $(u, v)$ for various $\varepsilon$, where the left side in each figure shows $u$ and the right side $v$.

chronous, and as $\varepsilon$ decreases the peaks of $u_h$ and $v_h$ becomes sharper and narrower. When $\varepsilon \to 0$, all of the peaks of $u$ and $v$ are located on a circle $\{(x, y)|x^2 + y^2 = 0.75^2\}$, with four peaks symmetrical about the origin consistent with the symmetry of system (1.1).

## 4. Conclusions

We have simulated the steady state coupled Schrödinger equations with the adaptive finite element method combined with damped Newton iteration. Our numerical results are summarised as follows.

1. For an elliptic domain and the homogeneous Neumann boundary condition, when $0 \leq \beta < \min\{\mu_1, \mu_2\}$ or $\beta > \max\{\mu_1, \mu_2\}$ the system (1.1) has two-spike synchronised solutions with both peaks located at the local maximum or minimum points of $H(P)$ — cf. items I and II in the section above. There also exist solutions with a peak located at one local maximum (or minimum) point of the $H(P)$, and we found that the segregated solution only occurs when $0 \leq \beta < \min\{\mu_1, \mu_2\}$ — cf. items III and IV. As $\varepsilon \to 0$, the maxima of $u_h$ and $v_h$ tend to constant values. These results are consistent with the theoretical results of Refs. [10, 13, 14]. We found an interior spike synchronised solution with peak located at a local maximum point of $dist(P, \partial\Omega)$ when $0 \leq \beta < \min\{\mu_1, \mu_2\}$ *or* $\beta > \max\{\mu_1, \mu_2\}$, as expected by many analysts — cf. item V. Under the homogeneous Dirichlet boundary condition, we found that when $0 \leq \beta < \min\{\mu_1, \mu_2\}$ or $\beta > \max\{\mu_1, \mu_2\}$ the system(1.1) has a least energy solution with peak located at a local maximum point of $dist(P, \partial\Omega)$ — cf. item VI. Our results are consistent with the theoretical results of Ref. [4].
2. For a dumbbell domain and the homogeneous Dirichlet boundary condition, when $0 \leq \beta < \min\{\mu_1, \mu_2\}$ *or* $\beta > \max\{\mu_1, \mu_2\}$ we found that the system (1.1) has synchronised least energy solutions with peaks located at one local maximum point of $dist(P, \partial\Omega)$, consistent with the theoretical results of Ref. [4] — cf. item VII. When $0 \leq \beta < \min\{\mu_1, \mu_2\}$ or $\beta > \max\{\mu_1, \mu_2\}$ the system (1.1) has two-spike synchronised solutions with peaks located at local maximum points of $dist(P, \partial\Omega)$, and we also found the system (1.1) has segregated solutions only when $0 \leq \beta < \min\{\mu_1, \mu_2\}$ in — cf. items VIII and IX. Some researchers have conjectured that these types of solutions occur, but no corresponding theoretical result has been obtained yet.

https://doi.org/10.4208/eajam.030616.130517a Published online by Cambridge University Press

3. For a circular ring domain, when $0 \leq \beta < \min\{\mu_1, \mu_2\}$ *or* $\beta > \max\{\mu_1, \mu_2\}$ we found that the system (1.1) has least energy solutions with a peak located at one local maximum point of $dist(p, \partial\Omega)$, consistent with the theoretical results of Ref. [4] — cf. item X. When $0 \leq \beta < \min\{\mu_1, \mu_2\}$ *or* $\beta > \max\{\mu_1, \mu_2\}$, we found that the system (1.1) has two-spike synchronised solutions with peaks located at two local maximum points of $dist(P, \partial\Omega)$, and also that a four-spike synchronised solution exists — cf. items XI and XII. Those solutions have been presumed to exist, but again there are as yet no corresponding theoretical results.

## Acknowledgments

The authors wish to thank Professor Zhengru Zhang for helpful discussions. One of us (G.J.) is partially supported by the National Natural Science Foundation of China (Grant Nos.11571045 and 11671052) and Fundamental Research Funds for central Universities (Grant No. 2015KJJCB23). Another of us (Z.T.) is partially supported by the National Natural Science Foundation (Grant No. 11571040), and another (H.Z.) by the National Natural Science Foundation of China (Grant No. 11471046).

## References

[1] B.D. Esry, C.H. Greene, J.P. Burke Jr. and J.L. Bohn, *Hartree-Fock theory for double condensates*, Phys. Rev. Letts. **78**, 3594-3597 (1997).
[2] E. Timmermans, *Phase separation of Bose-Einstein condensates*, Phys. Rev. Letts. **81**, 5718-5721 (1998).
[3] G. Chen, J. Zhou and W. Ni, *Algorithms and visualization for solutions of nonlinear elliptic equations*, Int. J. Bifurc. Chaos **10**, 1565-1612 (2000).
[4] T. Lin and J. Wei, *Spike in two coupled of nonlinear Schrödinger equations*, Ann. Inst. H. Poincaré Anal. Nonlin. **22**, 403-439 (2005).
[5] T. Lin and J. Wei, *Ground state of N coupled nonlinear Schrödinger equations in $R^n$, $n \leq 3$*, Comm. Math. Phys. **255**. 629-653 (2005).
[6] T. Lin and J. Wei, *Spike in two-component systems of nonlinear Schrödinger equations with trapping potentials*, J. Diff. Eq. **229**, 538-569 (2006).
[7] B. Sirakov, *Least energy solitary waves for a system of nonlinear Schrödinger equations in $R^n$*, Comm. Math. Phys. **271**, 199-221 (2007).
[8] T. Bartsch, Z.Q. Wang and J. Wei, *Bound states for a coupled Schrödinger systems*, J. Fixed Point Theory Appl. **2**, 353-367 (2007).
[9] N. Dancer and J. Wei, *Spike solutions in coupled nonlinear Schrödinger equations with attractive interaction*, Trans. Amer. Math. Soc. **361**, 1189-1208 (2009).
[10] Z. Tang, *Spike-layer solutions to singularly perturbed semilinear systems of coupled Schrödinger equations*, J. Math. Anal. Appl. **377**, 336-352 (2011).
[11] Z. Xie, Y. Yuan and J. Zhou, *On finding multiple solutions to a singularly perturbed Neumann problem*, SIAM J. Sci. Comput. **34**, A395-A420 (2012).
[12] S.J. Peng and Z.Q. Wang, *Segregated and synchronised vector solutions for nonlinear Schrödinger Systems*, Arch. Rational Mech. Anal. **208**, 305-339 (2013).
[13] Z. Tang, *Multi-peak solutions to a coupled Schrödinger system with Neumann boundary condition*, J. Math. Anal. Appl. **409**, 684-704 (2014).

https://doi.org/10.4208/eajam.030616.130517a Published online by Cambridge University Press

[14] Z. Tang, *Segregated peak solutions of coupled Schrödinger systems with Neumann boundary conditions*, Discrete Continuous Dyn. Systems **34**, 5299-5323 (2014).
[15] A. I.Ávila, A. Meister and M. Steigemann, *On numerical methods for nonlinear singularly perturbed Schrödinger problems*, Appl. Num. Math. **86**, 22-42 (2014).

https://doi.org/10.4208/eajam.030616.130517a Published online by Cambridge University Press